

ORIGINAL PAPER

C. M. Holl · J. R. Smyth · H. M. S. Laustsen
S. D. Jacobsen · R. T. Downs

Compression of witherite to 8 GPa and the crystal structure of BaCO₃II

Received: 10 September 1999 / Revised, accepted: 13 January 2000

Abstract Natural witherite (Ba_{0.99}Sr_{0.01}CO₃) has been studied by single-crystal X-ray diffraction in the diamond anvil cell at eight pressures up to 8 GPa. At ambient pressure, cell dimensions are $a = 5.3164(12)$ Å, $b = 8.8921(19)$ Å, $c = 6.4279(16)$ Å, and the structure was refined in space group $Pm\bar{c}n$ to $R(F) = 0.020$ from 2972 intensity data. The unit cell and atom position parameters for the orthorhombic cell were refined at pressures of 1.2, 2.0, 2.9, 3.9, 4.6, 5.5, 6.2, and 7.0 GPa. The volume-pressure data are used to calculate equation of state parameters $K_{T0} = 50.4(12)$ GPa and $K' = 1.9(4)$. At approximately 7.2 GPa, a first-order transformation to space group $P\bar{3}1c$ was observed. Cell dimensions of the high-pressure phase at 7.2 GPa are $a = 5.258(6)$ Å, $c = 5.64(1)$ Å. The high pressure structure was determined and refined to $R(F) = 0.06$ using 83 intensity data, of which 15 were unique. This high-pressure phase appears to be more compressible than the orthorhombic phase with an estimated initial bulk modulus ($K_{7.2\text{GPa}}$) of 10 GPa.

Key words Witherite · High pressure · Aragonite · Crystal structure

Introduction

Carbonate minerals and fluid phase CO₂ are thought to be minor components of the upper mantle. CO₂ is an important volatile component affecting stability fields and phase relations of mantle minerals and controlling the genesis of carbonatite and kimberlite magmas. In addition, shock heating of surface carbonate rocks that would occur in large meteorite impact events has the potential to cause a significant atmospheric CO₂ transient. Rates of devolatilization of carbonate minerals under these conditions depend greatly on the bulk moduli of these minerals (Tyburczy and Ahrens 1986).

There remain some major uncertainties about the high-pressure behavior of CaCO₃. Calcite is known to have two high-pressure polymorphs, known as calcite II (Merrill and Bassett 1975) and calcite III (Smyth and Ahrens 1997), which are produced by successive displacive transformations from calcite. The intermediate phase, calcite II, is more compressible than either calcite I or III. Both calcite II and calcite III are less dense than aragonite and so appear to be metastable relative to aragonite.

Shock compression studies of aragonite indicate a possible postaragonite phase (Vizgirda and Ahrens 1983), termed CaCO₃ VI, which occurred at pressures between 5.5 and 7.6 GPa at poorly constrained temperature. Neither the density nor structure of this phase could be inferred from these studies. Lin and Liu (1996, 1997) report a quenchable high-pressure phase of strontianite (SrCO₃), cerussite (PbCO₃), and witherite (BaCO₃) that was similar in each compound and appeared at pressures less than 4 GPa and temperatures of about 1000 °C. Raman spectroscopy indicated that the transition took place at 35, 17, and 8 GPa in SrCO₃, PbCO₃, and BaCO₃, respectively. From X-ray powder diffraction data taken on quenched samples, they inferred that the space group of the new phase (BaCO₃II) was $P2_122$ with a unit cell dimensionally similar to the aragonite forms of these minerals, but with

C. M. Holl · J. R. Smyth (✉) · H. M. S. Laustsen
S. D. Jacobsen
Department of Geological Sciences,
University of Colorado, Boulder, Colorado 80309-0399, USA

J. R. Smyth
Bayerisches Geoinstitut, Universität Bayreuth,
Bayreuth, 95447 Germany

R. T. Downs
Department of Geosciences, University of Arizona,
Tucson, Arizona 85721-0077, USA
E-mail: Joseph.smyth@colorado.edu
Fax: +1303 492 2606;
Tel.: +1303 492 5521

doubled a and b axes. They did not propose a structure or discuss any possible structural relations to the aragonite structure. The proposed cell bears an obvious relation to the aragonite-structure cell, so the transformation is likely to be displacive or at least epitaxial. Unless such a transformation involved chemical ordering, it is difficult to see how it could be preserved on quenching. Aragonite has been studied with powder X-ray diffraction in a cubic multi-anvil apparatus to pressures of 7 GPa and 1000 K (Martinez et al. 1996). At 298 K, the isothermal K_0 and K_0' of aragonite is 65.4(5) GPa and 2.7(7), respectively. No transformations were observed in aragonite over the pressure and temperature range studied.

In order to search for possible high-pressure modifications that might occur in aragonite, we have investigated the structure of witherite at pressures to 8 GPa at 300 K. Witherite was chosen for this study because it is isostructural with aragonite, which is a major carbonate phase of geophysical interest. The cation radius of Ba is greater than that of the divalent cations of the other members of the group, so that any pressure-induced phase transformations that occur in aragonite should also occur in witherite, but at lower pressures (Prewitt and Downs 1998; Weinbruch et al. 1992). Indeed, Lin and Liu (1997) observed a transformation in this phase at 8 GPa, within the range of our single-crystal diamond anvil cells.

Carbonates of the aragonite group crystallize in space group $Pm\bar{c}n$ and consist of layers of nine-coordinated metal atoms in approximate hexagonal closest packing, alternating with layers of carbonate groups perpendicular to the c -axis (DeVilliers 1971). The aragonite structure can be described as a distorted trigonal structure, and the mineral often displays pseudo-hexagonal crystals, as does witherite. This structure is depicted in Fig. 1. Witherite is the member of this group whose structure is closest to ideal (Speer 1983).

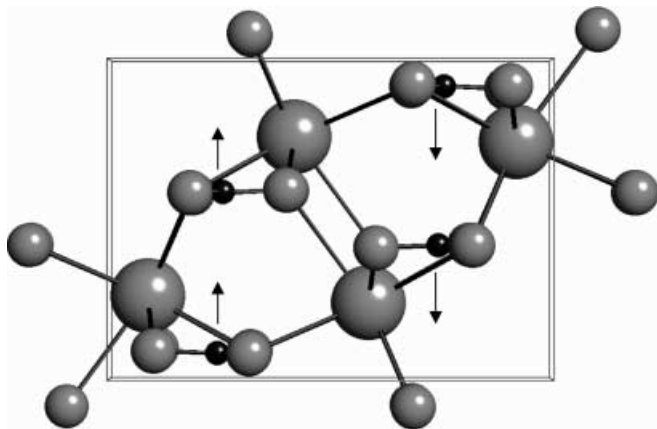


Fig. 1 Illustration of the witherite (BaCO_3) structure. Large spheres represent Ba, intermediate spheres represent O, and the smallest spheres represent C. Arrows indicate the direction of motion of the carbonate groups upon compression as the structure approaches the trigonal phase

In order to understand the high-pressure crystal chemistry of aragonite-group carbonates, we investigated the structure of witherite at high pressure and ambient temperature by single-crystal X-ray diffraction in the diamond anvil cell. Our objectives were to measure the bulk modulus of witherite, to observe the mechanisms of compression by structure refinements at pressure, and to characterize the postaragonite structure at pressure, if observed.

Experimental

The X-ray diffraction instrument used throughout this study was a Siemens four-circle diffractometer with an 18-kW generator, Mo rotating anode, and incident-beam horizontal graphite monochromator. Because the horizontal graphite monochromator always causes variations in the intensity ratio of $K\alpha_1$ and $K\alpha_2$ and hence the effective wavelength of the unresolved peak, the wavelength of the combined $K\alpha_1$ and $K\alpha_2$ is calibrated using a ruby standard crystal. Wavelength calibrations were run between all unit cell measurements and data collections. Structure refinements were performed using SHELXTL (Sheldrick 1990) using neutral-atom scattering factors. Polyhedral volume calculations were done using VOLCAL (Hazen and Finger 1982).

The diamond anvil cell used for this study was a miniature Merrill–Bassett type constructed of Vascomax 600 steel, which uses low-profile diamonds with 500- μm culet faces (Merrill and Bassett 1974). The cell has hardened Vascomax 900 steel seats that give an open aperture of 60°. The Re gasket was precompressed from an initial 250 μm to a thickness of 100 μm , and a 250- μm hole was machined at the center of the indentation, to serve as the pressure chamber. The pressure medium was methanol, ethanol, and water (16:3:1), which remains an isotropic liquid throughout the pressure range studied (Chai and Brown 1996). Pressure was determined by the ruby fluorescence method (Piermarini et al. 1975; Mao et al. 1986). The ruby fluorescence spectrometer uses an Ar ion laser in transmission mode and one of the Ar plasma emission lines for wavelength calibration. Peak fitting was done using a locally written Gaussian and Lorentzian peak-fitting routine. At each pressure studied, the cell was allowed to equilibrate for a minimum of 18 h before cell determination and data collection. The pressure was measured before and after each data collection.

Natural witherite (University of Colorado Collection Number 5914) from Hexham, Northumberland, England was used for this study. Chemical analysis by energy-dispersive X-ray spectroscopy

Table 1 Cell parameters of orthorhombic witherite and the trigonal high-pressure witherite

P (GPa)	a (Å)	b (Å)	c (Å)	V (Å ³)	Molar vol (cm ³) ³
Witherite					
0.00	5.316(1)	8.892(2)	6.428(2)	303.76(12)	45.73(2)
1.26(5)	5.300(1)	8.868(2)	6.318(1)	296.94(10)	44.70(2)
1.98(5)	5.292(1)	8.856(2)	6.246(2)	292.69(12)	44.06(2)
2.95(5)	5.282(1)	8.843(2)	6.148(1)	287.15(10)	43.23(2)
3.94(5)	5.274(1)	8.838(2)	6.060(1)	282.44(11)	42.52(2)
4.56(5)	5.269(1)	8.838(2)	5.999(1)	279.31(10)	42.05(2)
5.50(5)	5.260(1)	8.846(2)	5.895(2)	274.29(12)	41.29(2)
6.20(5)	5.255(1)	8.852(2)	5.838(1)	271.58(11)	40.89(2)
7.05(5)	5.251(1)	8.868(2)	5.762(2)	268.05(15)	40.35(2)
Trigonal post-witherite phase					
7.20(5)	5.258(6)		5.64(1)	135.0(5)	40.64(15)
7.50(5)	5.229(8)		5.48(2)	129.7(6)	39.05(18)
8.20(5)	5.19(2)		5.30(5)	123.7(10)	37.3(3)

indicated a composition of approximately $(\text{Ba}_{0.99}\text{Sr}_{0.01})\text{CO}_3$. No elements other than Ba and Sr were observed in the spectra. A roughly equant single-crystal fragment approximately 200 μm across was used for the ambient pressure study. Cell parameters were obtained by least-squares analysis of angular positions of 52 reflections. This dataset included two-position ($\pm 2\theta$) centering of 26 unique reflections with $2\theta < 25^\circ$. Unit cell parameters are presented in Table 1.

X-ray intensity data comprising a hemisphere of reciprocal space ($\pm h \pm k + l$) were measured at ambient conditions using θ - 2θ scans and scan speeds variable from 4 to $20^\circ 2\theta \text{ min}^{-1}$. This resulted in 2972 reflection intensity data, of which 700 were unique and greater than 3σ in intensity. The data were corrected for Lorentz and polarization effects and for absorption using an analytical absorption correction routine in SHELXTL. The calculated absorption coefficient, μ , was 12.85 mm^{-1} . Absorption correction reduced the R of merging of equivalent reflections from 0.036 to 0.014. Using anisotropic displacement parameters for all atoms, the final R for 2972 observed reflections converged to 0.020. The weighted R was 0.019. Details of the room pressure intensity data and structure refinement are listed in Table 2, final model atom positions in Table 3, displacement parameters in Table 4, and selected interatomic distances in Table 5.

For high-pressure studies, a crystal fragment was selected for clarity and low mosaicity and oriented using X-ray precession photography. In order to optimize the number of accessible diffraction data in the diamond anvil cell, a specific orientation was selected. The crystal was mounted on a slide parallel to (1 1 1), flattened and polished to a thin section approximately 40 μm in thickness. Fragments were photographed by X-ray precession to insure they were not twinned or damaged during preparation. Fragments of this crystal were loaded into a Merrill-Bassett-type miniature diamond anvil cell. Three separate loads of the diamond cell were analyzed; data presented here were obtained from the second load because the crystal quality was greatest. The unit cell parameters were refined at each pressure based on two-position centering of 13 unique reflections with $2\theta < 25^\circ$. These data are compiled in Table 1.

X-ray intensity data were measured at each pressure using θ - 2θ scans in bisecting mode. Diamond cell geometry restricted the number of accessible reflections for high pressure structure refinements to approximately 170. Intensity data were corrected for Lorentz and polarization effects and for absorption of the DAC using DACABS (R.T. Downs 1997, personal communication). Equivalent intensities were averaged and intensities that were obstructed by the cell were omitted. Structure refinement and data collection parameters are presented in Table 2. Final atom position and isotropic displacement parameters of witherite in *Pmcn* at each pressure are given in Table 3.

During the first run, a transformation was observed at approximately 7.5 GPa. However, no reflections were observed above this pressure based on a long exposure rotation photograph. The pressure was then released and the sample removed from the cell. An X-ray precession photograph of the crystal showed powder lines of witherite, although the extra reflections reported by Lin and Liu (1997) would probably be too weak to be observed by this method. In the second and third sample runs, this transformation was observed at 7.2 GPa and was marked by a loss of the orientation reflections. A rotation photograph showed a new set of reflections, which were significantly broader than those of the initial phase. Least-squares analysis of the angular positions of 24 reflections at 7.2 GPa in the second run gave trigonal or hexagonal unit cell parameters of $a = b = 5.258(6) \text{ \AA}$, $c = 5.64(1) \text{ \AA}$. The c - and a -axial directions of the new cell were approximately those of the orthorhombic cell. The unit cell parameters of the high-pressure phase were measured at 7.5 and 8.2 GPa. These data are reported in Table 1. At the highest pressure, the reflections became weak and diffuse so that only eight unique reflections were successfully centered.

Eighty-three reflection intensity data were measured from the posttransformation phase. Systematic extinctions of this phase were consistent with space groups $P\bar{3}1c$ and $P31c$. Averaging of

reflections equivalent in either of these space groups gave an R of merging of 0.019. Assuming the centric space group, a model was constructed based on the presumed epitaxial relation of the new cell to the orthorhombic cell and the symmetry constraints of the apparent trigonal space group. The oxygen position parameter and isotropic displacement parameters for Ba were refined in this space group using 15 unique data to $R(F) = 0.059$ with weighted $R(F)$ of 0.038. Given the success of the centric model and the small number of observed data, no attempt was made to model the structure in the acentric space group.

Atom positions for the trigonal high-pressure postwitherite phase at 7.2 GPa are given in Table 6. The structure of the phase consists of planes perpendicular to the c -axis containing both the Ba atoms and the carbonate groups. These planes are constrained by symmetry to occur at $z/c = 1/4$ and $3/4$. Ba is in 12-fold coordination with six oxygen atoms in the same plane each at about $2.65(3) \text{ \AA}$ distant and three oxygen atoms in each of the adjacent planes, each at about $3.32(3) \text{ \AA}$ distant. The C-O distance is $1.27(2) \text{ \AA}$. The structure is depicted in Fig. 2. The posttransformation phase is epitaxial to witherite with respect to the c - and a -axes. Additional cell parameters of the trigonal phase were obtained at 7.5 and 8.2 GPa during the second run (Table 1). From these, we roughly estimate that the bulk modulus K_T of the trigonal phase at 7 GPa is about 10 GPa, and so it appears considerably more compressible than witherite, at least at pressures near the transformation.

Discussion and conclusions

Ambient pressure unit cell parameters and atomic positional parameters (Table 1) are in statistical agreement with those obtained by DeVilliers (1971). Errors on the positional parameters indicate a significant improvement over the previous refinement by a factor of about 4. DeVilliers (1971) reported a displacement of 0.07 \AA of the carbon atom out of the plane of the carbonate oxygens. Our observation is that the C is about $0.017(2) \text{ \AA}$ out of the plane. Deviation of the carbonate groups from the normal to the c -axis was found to be $1.44(4)^\circ$, very similar to the 1.5° reported by DeVilliers (1971).

Unit cell parameters determined at each pressure are presented in Table 1 and plotted in Fig. 3. Compression of the structure is strongly anisotropic, with the axial strain along c (normal to the carbonate groups) being approximately ten times that along a and b . The b -axis length reaches a minimum at 4.2 GPa, and increases with increasing pressure beyond this point. The other axes showed a roughly linear decrease in length with increasing pressure.

Equation of state parameters for witherite were determined by fitting the volume-pressure data to a third-order Birch-Murnaghan equation of state (Birch 1947, 1978). Writing pressure as the dependent variable, we calculate a three-parameter (V_0 , K_{T0} , K') weighted least-squares fit to the data using a weighting scheme based on the actual uncertainties in the pressure and volume measurements (Angel et al. 1997). This results in EOS parameters $V_0 = 303.82(14) \text{ \AA}^3$, $K_{T0} = 50.4(12) \text{ GPa}$, and $K' = 1.9(4)$. The pressure versus molar volume data and EOS fit are plotted in Fig. 4. Note that the EOS zero-pressure volume is very close to the experimental value $V_0 = 303.76(2) \text{ \AA}^3$. The bulk

Table 2 Number of observed intensity data and model statistics for high-pressure refinements of witherite

	<i>P</i> (GPa)									
	0.0	1.26	1.98	2.95	3.94	4.56	5.50	6.20	7.05	7.2
Total reflections	2972	164	167	171	184	178	170	170	170	83
Unique and >3 σ	700	42	39	43	40	40	38	38	37	15
Data merging (R)	0.014	0.008	0.001	0.001	0.014	0.015	0.020	0.030	0.006	0.019
R(F)	0.020	0.029	0.030	0.028	0.021	0.027	0.024	0.025	0.039	0.059
WR(F)	0.019	0.023	0.024	0.025	0.017	0.022	0.021	0.024	0.023	0.038

Table 3 Structure of witherite at ambient and high pressures

	<i>P</i> (GPa)									
	0.00	1.26	1.98	2.95	3.94	4.56	5.50	6.20	7.05	
Ba										
<i>x/a</i>	1/4	1/4	1/4	1/4	1/4	1/4	1/4	1/4	1/4	1/4
<i>y/b</i>	0.41631(2)	0.4161(3)	0.4159(3)	0.4165(4)	0.4165(2)	0.4165(3)	0.4167(3)	0.4165(4)	0.4168(4)	
<i>z/c</i>	0.75462(2)	0.7557(7)	0.7553(7)	0.7554(6)	0.7559(4)	0.7562(5)	0.7557(5)	0.7560(6)	0.7551(4)	
<i>U</i> _{iso}	0.00914(5)	0.011(2)	0.015(2)	0.012(1)	0.011(1)	0.011(1)	0.011(1)	0.010(2)	0.011(2)	
C										
<i>x/a</i>	1/4	1/4	1/4	1/4	1/4	1/4	1/4	1/4	1/4	
<i>y/b</i>	0.7563(3)	0.758(10)	0.757(10)	0.765(8)	0.752(4)	0.756(5)	0.760(5)	0.762(9)	0.768(7)	
<i>z/c</i>	0.9197(3)	0.925(11)	0.916(12)	0.904(9)	0.905(6)	0.906(8)	0.899(9)	0.895(11)	0.905(12)	
<i>U</i> _{iso}	0.0105(5)	0.051(16)	0.048(17)	0.012(10)	0.017(7)	0.016(9)	0.017(9)	0.021(12)	0.011(10)	
O(1)										
<i>x/a</i>	1/4	1/4	1/4	1/4	1/4	1/4	1/4	1/4	1/4	
<i>y/b</i>	0.9010(2)	0.903(4)	0.899(4)	0.904(4)	0.901(2)	0.905(3)	0.901(3)	0.901(5)	0.900(5)	
<i>z/c</i>	0.9115(3)	0.907(7)	0.894(6)	0.897(7)	0.894(4)	0.891(5)	0.892(6)	0.883(7)	0.875(6)	
<i>U</i> _{iso}	0.0158(5)	0.017(8)	0.021(6)	0.022(7)	0.014(6)	0.011(6)	0.015(7)	0.011(8)	0.015(7)	
O(2)										
<i>x/a</i>	0.4596(3)	0.462(3)	0.460(2)	0.459(2)	0.461(2)	0.460(2)	0.461(2)	0.462(3)	0.460(2)	
<i>y/b</i>	0.6841(2)	0.683(3)	0.680(4)	0.684(3)	0.678(3)	0.680(3)	0.684(3)	0.682(4)	0.684(3)	
<i>z/c</i>	0.9194(2)	0.927(5)	0.918(4)	0.911(4)	0.910(4)	0.908(3)	0.903(4)	0.900(4)	0.892(5)	
<i>U</i> _{iso}	0.0156(3)	0.014(5)	0.022(6)	0.014(5)	0.012(4)	0.009(4)	0.011(4)	0.013(5)	0.014(4)	

Table 4 Anisotropic atomic displacement parameters for witherite at ambient pressure

Atom	U ₁₁	U ₂₂	U ₂₃	U ₁₂	U ₁₃	U ₂₃
Ba	0.00867(9)	0.00871(9)	0.01004(9)	0.00	0.00	0.00045(5)
C	0.0115(9)	0.0115(9)	0.0086(8)	0.00	0.00	-0.0016(8)
O1	0.0170(9)	0.0101(7)	0.0201(9)	0.00	0.00	-0.0016(7)
O2	0.0110(5)	0.0142(6)	0.0216(6)	0.0025(5)	-0.0022(5)	0.0013(5)

Table 5 Cation-oxygen bond distances in witherite at ambient and high pressures

	<i>P</i> (GPa)									
	0.00	1.26	1.98	2.95	3.94	4.56	5.50	6.20	7.05	
Ba-O1 (×1) (Å)	2.739(2)	2.73(4)	2.783(38)	2.677(43)	2.722(23)	2.699(29)	2.682(34)	2.708(41)	2.725(43)	
Ba-O1 (×2)	2.868(1)	2.845(17)	2.811(14)	2.820(16)	2.793(8)	2.781(10)	2.773(12)	2.754(11)	2.734(11)	
Ba-O2 (×2)	2.752(1)	2.668(25)	2.689(26)	2.712(24)	2.669(16)	2.666(18)	2.674(21)	2.657(23)	2.691(24)	
Ba-O2 (×2)	2.810(1)	2.817(25)	2.810(29)	2.761(25)	2.788(20)	2.775(20)	2.724(22)	2.728(28)	2.698(23)	
Ba-O2 (×2)	2.834(1)	2.835(27)	2.781(32)	2.782(27)	2.729(21)	2.731(22)	2.753(24)	2.732(30)	2.732(25)	
Average	2.807	2.784	2.774	2.759	2.742	2.734	2.726	2.717	2.715	
poly. vol. (Å ³)	50.97	49.59	49.36	48.66	47.66	47.32	46.69	46.38	46.31	
C-O1 (×1)	1.288(3)	1.31(9)	1.27(9)	1.23(8)	1.31(4)	1.32(5)	1.25(6)	1.23(9)	1.19(8)	
C-O2 (×2)	1.286(2)	1.30(5)	1.31(5)	1.32(4)	1.29(2)	1.30(3)	1.30(3)	1.32(5)	1.33(4)	
Average	1.287	1.30	1.30	1.29	1.30	1.31	1.28	1.29	1.26	

Table 6 Atom position parameters of high-pressure trigonal witherite in space group $P-31c$ at 7.2 GPa

Atom	x/a	y/b	z/c
Ba	2/3	1/3	1/4
C	0	0	1/4
O	0.140(5)	0.860(5)	1/4

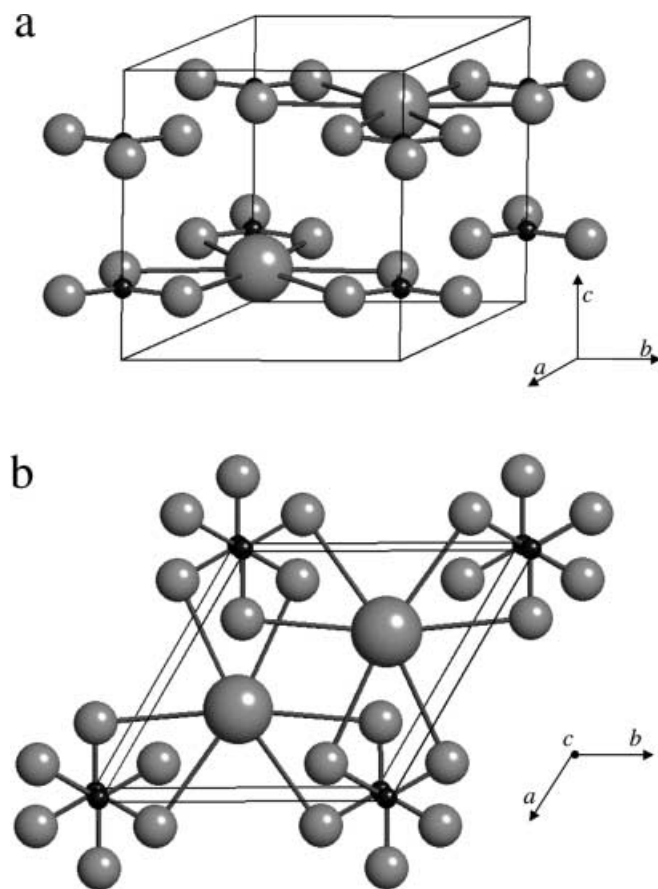


Fig. 2 c -axis (a) and a -axis (b) projections of the postwitherite, trigonal phase observed at 7.2 GPa

modulus corresponds to compressibility at low pressures of $1.98(4) \text{ Mbar}^{-1}$, in agreement with the $2.0(1) \text{ Mbar}^{-1}$ obtained by Martens et al. (1982) over the range of 0 to 7 kbar. The bulk modulus of the high-pressure trigonal phase is approximately 10 GPa at 7.2 GPa pressure if we assume K' to be in the range of 2 to 4. The very slight increase in molar volume at the transition apparent in Fig. 4 could be due either to experimental uncertainty or to a slight hysteresis in the transition.

The structure parameters were refined at each pressure to identify trends and to determine the pressure at which the orthorhombic-trigonal transformation occurred. Along with decreasing Ba-O polyhedral volumes and bond lengths, a trend was seen in which the z/c positional coordinates of the carbonate groups changed with increasing pressure. Movement of the carbonate groups was toward the planes occupied by the Ba atoms,

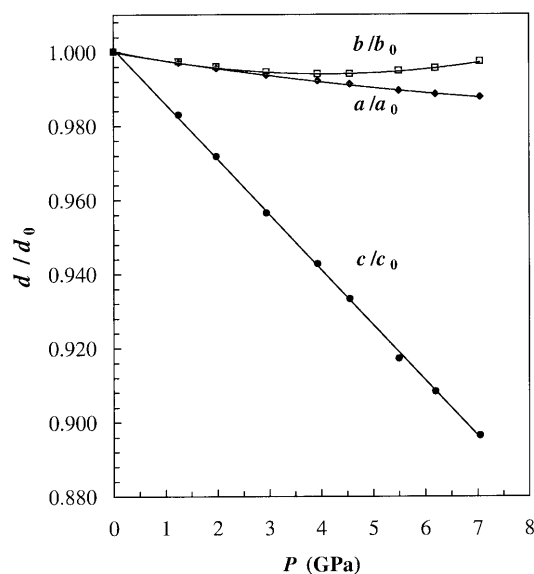


Fig. 3 Axial compression of the unit-cell of witherite plotted with d/d_0 as a function of pressure (GPa). The solid curves are of no physical significance

which moved little relative to the unit-cell symmetry operators. This trend is illustrated in Fig. 1. As described above, the compression of the structure is observed as shortening of the c -axis, perpendicular to the alternating planes of cations and carbonate groups. With increasing pressure, the carbonate groups move along the c -axis toward the plane of the Ba atoms. Also, the carbonate groups show a significant tilt out of the plane normal to c at room pressure. This is possibly due to Ba-O1 repulsion as this is the shortest barium-oxygen bond. The amount of tilt appears to increase with pressure as the short Ba-O1 distance shows little variation (Table 5).

Evidence for a first-order phase transformation at approximately 7.2 GPa in the second and third runs appears to be conclusive. First, the positions of the reflections changed abruptly, requiring a new orientation photograph and a new matrix. Second, the peaks seen upon centering these reflections were less intense by about an order of magnitude and covered a broader angular range than peaks seen below the transformation. Third, analysis of peak-position data indicates trigonal, rather than orthorhombic, symmetry. Fourth, the compressibility of the material increased significantly above this pressure. Additionally, the lengthening of the b -axis with increasing pressure above 4.2 GPa is consistent with the structure's approach to trigonal symmetry with $a/b = 3^{1/2}$. Finally, quenched samples were polycrystalline in all cases. The discontinuities in these trends indicate a displacive transformation occurring at this point; however, the abruptness of the changes gives the appearance of a first-order transformation.

The question remains as to whether the high-pressure structure observed in this study actually represents the same postaragonite phase observed in shock compression

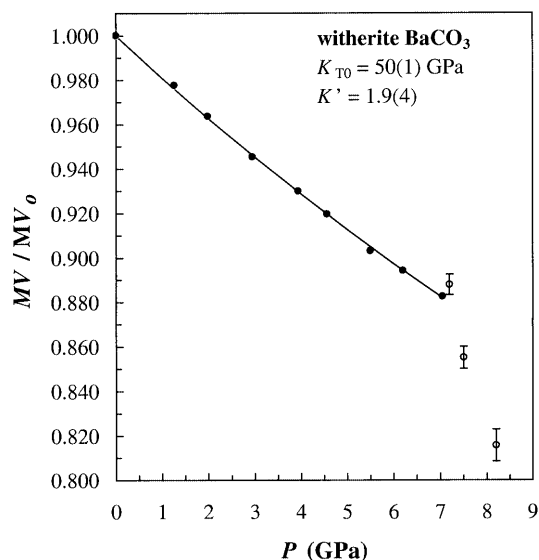


Fig. 4 Molar volume compression of witherite BaCO_3 plotted as MV/MV_0 as a function of pressure (GPa) to show both the orthorhombic and trigonal phases. The solid curve represents the fitted second-order Birch-Murnaghan equation of state for the orthorhombic phase

of aragonite by Vizgirda and Ahrens (1982) and in static compression of SrCO_3 , PbCO_3 , and BaCO_3 by Lin and Liu (1996, 1997). The reasonable nearest-neighbor distances and high coordination number of the high-pressure phase, together with the relatively low R factors, give confidence that the structure is indeed correct. Further, refinements of the orthorhombic structure at pressure show the carbonate groups moving closer to the planes of the Ba atoms with increasing pressure until they occupy the same planes as Ba after the transformation. However, the apparent very low bulk modulus of the structure near the phase transition seems to indicate that the structure observed in the present study may be transitory to a different structure occurring at higher pressure. This would be consistent with the broadening and weakening of the X-ray reflections observed at pressures above 8 GPa.

The oxygen and barium atoms in the low-pressure witherite structure are arranged in a very distorted hexagonal-close-packed (HCP) array with puckered monolayers. In the high-pressure structure, the array is still HCP, but the monolayers are no longer puckered. The high-symmetry, reasonable interatomic distances are consistent with the structure being stable over a considerable range of pressure and temperature. The short Ba-O distances in the a - b plane and long Ba-O distances out of the plane are also consistent with its having a very high initial compressibility in the c -direction. Once the carbonate groups are in the same plane as the Ba, there would be little resistance to further compression parallel to c for some range upwards in pressure. Further, the epitaxial relationship to the aragonite structure would most likely result in very fine-scale twinning and shear in the quenched samples. This may help to account for the low symmetry and high strain observed in the quenched

samples (Lin and Liu 1997). It would appear likely, then, that the observed structure is indeed the postaragonite phase, and that the low-symmetry phase reported by Lin and Liu (1996, 1997) is a metastable, kinetic remnant of the high-symmetry, high-pressure form.

The epitaxial relation of the high-pressure phase to the precursor orthorhombic phase and the very large compressional anisotropy may also account for the anomalous heating observed in shock compression studies of carbonates (Tyburczy and Ahrens 1986; Kondo and Ahrens 1983). Lin and Liu (1996) observed similar transformations in PbCO_3 at 17 GPa and SrCO_3 at 35 GPa at room temperature. Extrapolating this trend with divalent cation radius, they estimated a 300-K transformation pressure of 130 GPa for CaCO_3 . However, they postulated that the Clapeyron slope of the reaction was negative based on observations of the transformation as low as 4 GPa at 1000 °C. A negative Clapeyron slope would then be consistent with the higher temperature and pressure phase having higher symmetry. A negative Clapeyron slope would put the transition within the pressure range of shock experiments for CaCO_3 .

In conclusion, we have investigated the compressibility and high-pressure polymorphism of witherite (BaCO_3), an aragonite-group carbonate. The structure shows continuous compression behavior to 7.2 GPa with an apparent bulk modulus (K_{T0}) of 50.4(9) GPa and K' of 1.9(3) over this range. The c -axis of the orthorhombic structure is approximately ten times more compressible than a or b as the carbonate groups approach the plane of the Ba atoms. At 7.2 GPa there is a displacive, first-order transformation to space group $P\bar{3}1c$. The structure of the high-pressure, postaragonite form (BaCO_3 -II) has been determined and refined to an $R(F)$ of 0.06. It is a new carbonate structure consisting of coplanar Ba and carbonate groups. The high-pressure form is more compressible than the low-pressure form which is consistent with its having short Ba-O distances in the a - b plane and long distances out of the plane. As with other carbonates, the elastic behavior is highly anisotropic.

Acknowledgements This work was supported by the National Science Foundation through grant EAR 97-25672 and in part by a *Deutsche Forschungsgemeinschaft* Visiting Professorship at *Bayrisches Geoinstitut* to J.R. Smyth.

References

- Angel RJ, Allan DR, Miletich R, Finger LW (1997) The use of quartz as an internal pressure standard in high-pressure crystallography. *J Appl Cryst* 30: 461-466
- Birch F (1947) Finite elastic strain of cubic crystals. *Phys Rev* 71: 809-824
- Birch F (1978) Finite strain isotherm and velocities for single-crystal and polycrystalline NaCl at high pressure and 300 K. *J Geophys Res* 83: 1257-1268
- Chai M, Brown JM (1996) Effects of non-hydrostatic stress on the R lines of ruby single crystals. *Geophys Res Lett* 24: 3539-3542
- DeVilliers JPR (1971) Crystal structures of aragonite, strontianite, and witherite. *Am Mineral* 56: 759-767

- Hazen RM, Finger LW (1982) Comparative crystal chemistry; temperature, pressure, composition and the variation of crystal structure. Wiley, New York, 231 pp
- Kondo K, Ahrens TJ (1983) Heterogeneous shock-induced thermal radiation in minerals. *Phys Chem Mineral* 9: 173–181
- Lin CC, Liu LG (1996) Post-aragonite phase transitions in strontianite and cerussite – a high-pressure Raman spectroscopic study. *J Phys Chem Solids* 58: 977–987
- Lin CC, Liu LG (1997) High pressure phase transformations in aragonite-type carbonates. *Phys Chem Mineral* 24: 149–157
- Martens R, Rosenhauer M, v Gehlen K (1982) Compressibilities of carbonates. In: Schreyer W, (ed) *High Pressure Research in Geophysics*. E. Schweizerbart'sche Verlagsbuchhandlung, Stuttgart, 215–222
- Martinez I, Zhang J, Reeder RJ (1996) In situ X-ray diffraction of aragonite and dolomite at high pressure and high temperature: evidence for dolomite breakdown to aragonite and magnesite. *Am Mineral* 81: 611–624
- Merrill L, Bassett WA (1974) Miniature diamond anvil cell for single crystal X-ray diffraction studies. *Rev Sci Instr* 45: 290–294
- Merrill L, Bassett WA (1975) The crystal structure of $\text{CaCO}_3(\text{II})$, a high pressure metastable phase of calcium carbonate. *Acta Cryst* 31: 343–349
- Mao HK, Xu J, Bell PM (1986) Calibration of the ruby pressure gauge to 800 kbar under quasi-hydrostatic conditions. *J Geophys Res* 91: 4673–4676
- Piermarini GJ, Block S, Barnet JD, Forman RA (1975) Calibration of the pressure dependence of the R_1 ruby fluorescence line to 195 kbar. *J Appl Phys* 46: 2774–2780
- Prewitt CT, Downs RT (1998) High-pressure crystal chemistry. *Rev Mineral* 37: 283–318
- Sheldrick G (1990) SHELXTL-PC (Release 4.1) Siemens analytical X-ray instruments Inc, Madison, Wisconsin, 296 pp
- Smyth JR, Ahrens T (1997) The crystal structure of calcite III. *Geophys Res Lett* 25: 1595–1598
- Speer JA (1983) Crystal chemistry and phase relations of the orthorhombic carbonates. *Rev Mineral* 11: 164–189
- Tyburczy J, Ahrens T (1986) Dynamic compression and volatile release of carbonates. *J Geophys Res* 91: 4730–4744
- Vizgirda J, Ahrens T (1982) Shock compression of aragonite and implications for the equation of state of carbonates. *J Geophys Res* 87: 4747–4758
- Weinbruch S, Büttner H, Rosenhauer M (1992) The orthorhombic-hexagonal phase transformation in the system $\text{BaCO}_3\text{-SrCO}_3$ to pressures of 7000 bar. *Phys Chem Mineral* 19: 289–297